CORA Cork Open Research Archive
Cartlann Taighde Oscailte Chorcaí

Title	3D printed rechargeable aqueous and non-aqueous lithium-ion batteries: Evolution of design and performance
Authors	Egorov, Vladimir;Gulzar, Umair;O'Dwyer, Colm
Publication date	2023-12-12
Original Citation	Egorov, V., Gulzar, U. and O'Dwyer, C. (2023) '3d printed rechargeable aqueous and non-aqueous lithium-ion batteries: evolution of design and performance', ECS Advances, 2(4), 040508 (10 pp). Available at: https://doi.org/10.1149/2754-2734/ad120c.
Type of publication	Article (peer-reviewed)
Link to publisher's version	10.1149/2754-2734/ad120c
Rights	© 2023 The Author(s). Published on behalf of The Electrochemical Society by IOP Publishing Limited. This is an open access article distributed under the terms of the Creative Commons Attribution 4.0 License (CC BY, http://creativecommons.org/licenses/by/4.0/), which permits unrestricted reuse of the work in any medium, provided the original work is properly cited. [DOI: 10.1149/2754-2734/ad120c] - http://creativecommons.org/licenses/by/4.0/
Download date	2026-11-08 12:08:10
Item downloaded from	https://hdl.handle.net/10468/15834

UCC
University College Cork, Ireland
Coláiste na hOllscoile Corcaigh

ECS Advances

The Electrochemical Society
Advancing solid state & electrochemical science & technology

OPEN ACCESS

3D Printed Rechargeable Aqueous and Non-Aqueous Lithium-Ion Batteries: Evolution of Design and Performance

To cite this article: Vladimir Egorov *et al* 2023 *ECS Adv.* **2** 040508

View the article online for updates and enhancements.

You may also like

- High-Performance Organic Field-Effect Transistors Based on Two-Dimensional Vat Orange 3 Crystals
Ning Yan, , Zhiren Xiong et al.
- Vat Orange 11—Based Organic Cathode Material for High Rate Rechargeable Magnesium Battery
Tripathy Debashis, H. M. Viswanatha, M. N. K. Harish et al.
- *(Invited)* The Importance of Characterizing and Calibrating Light Engines in Vat Photopolymerization Additive Manufacturing
Benjamin Caplins



Your Lab in a Box!
The PAT-Tester-i-16: All you need for Battery Material Testing.
All-in-One Solution with integrated Temperature Chamber!
Cableless Connection for Battery Test Cells!
Fully featured Multichannel Potentiostat / Galvanostat / EIS!
www.el-cell.com +49 40 79012-734 sales@el-cell.com
EL-CELL®
electrochemical test equipment

This content was downloaded from IP address 109.78.119.40 on 29/04/2024 at 09:55

ECS Advances, 2023 **2** 040508

3D Printed Rechargeable Aqueous and Non-Aqueous Lithium-Ion Batteries: Evolution of Design and Performance

Vladimir Egorov,[1] Umair Gulzar,[1] and Colm O'Dwyer[1,2,3,*,z]

[1]*School of Chemistry, University College Cork, Cork T12 YN60, Ireland*
[2]*AMBER Research Centre, Trinity College Dublin, Dublin 2, Ireland*
[3]*Environmental Research Institute, University College Cork, Cork T23 XE10, Ireland*

Here we describe the modeling and design evolution of vat polimerized (Vat-P) stereolithographic apparatus (SLA) 3D printed coin cell-type aqueous and non-aqueous rechargeable lithium-ion batteries, cases and current collectors. We detail the rationale for design evolution that improved performance, handling and assembly of the printed batteries. Some guidance into the modeling, 3D printing process, material choice, chemical and electrochemical stability, assembly, sealing, and performance of 3D printed Li-ion batteries is outlined. 3D printed Li-ion batteries demonstrated promising results in terms of gravimetric capacity, rate capability, and capacity per unit footprint area compared to conventional coin cells in both aqueous and non-aqueous systems. For aqueous cells, the cell level capacity is a factor of 2–3x higher than similar metal coin cells due to the lighter weight and better rate response. We also outline design requirements for a Vat-P printed battery that are compatible with organic carbonate-based electrolytes, where the cell provides 115 mAh g^{-1} specific capacity using an $LiCoO_2$–graphite chemistry, which is only ~20% less than the maximum reversible capacity of LCO. Despite the challenges faced in optimizing the design and materials for 3D printed Li-ion batteries, this study provides valuable information for future research and development.

© 2023 The Author(s). Published on behalf of The Electrochemical Society by IOP Publishing Limited. This is an open access article distributed under the terms of the Creative Commons Attribution 4.0 License (CC BY, http://creativecommons.org/licenses/by/4.0/), which permits unrestricted reuse of the work in any medium, provided the original work is properly cited. [DOI: 10.1149/2754-2734/ad120c]

Manuscript received September 18, 2023. Published December 12, 2023.

The continuous demand for portable and sustainable energy storage systems has driven the rapid evolution of lithium-ion batteries (LIBs) in recent years. With the increasing demand for electric vehicles, smart grids, and wearable electronics, LIBs have emerged as one of the most reliable and efficient power sources.[1,2] However, the quest for developing high-performance LIBs with improved energy density, reduced manufacturing costs, and enhanced safety has intensified, requiring innovative solutions. One such technology that holds a lot of potential in transforming the field of energy storage is additive manufacturing (AM) or 3D printing.

Additive manufacturing has shown promising advancements in various fields, including aerospace, automotive, medical, and electronics, due to its ability to fabricate complex structures with high precision.[3] Its application in lithium-ion battery production is no exception, as 3D printing offers several advantages over conventional manufacturing techniques, such as reduced waste generation, lower cost, and customizable geometries.[4,5]

The types of 3D printed lithium-ion batteries vary significantly, depending on the application, performance requirements, and size constraints. Commonly used form factors include cylindrical, prismatic, pouch, and coin cell types. Common electrode configurations include in-plane and sandwich-type; each of them can incorporate thin-film, three-dimensional lattice, or interdigitated electrodes. Each type has its unique set of advantages and challenges, which may dictate the choice of materials, electrode configuration, and 3D printing techniques employed.[6,7]

Materials play a crucial role in determining the overall performance and safety of LIBs. For instance, choosing the right anode and cathode materials directly impacts the energy density, cycle life, and rate capability of the batteries. Conventional LIBs typically employ graphite as the anode material and a mixed lithium—transition metal oxide, such as lithium cobalt oxide ($LiCoO_2$) as the cathode material. However, recent advancements in materials science have led to the development of alternative anode materials, such as silicon (Si), tin (Sn), and their alloys, as well as novel cathode materials like lithium iron phosphate ($LiFePO_4$) and lithium nickel manganese cobalt oxide ($LiNiMnCoO_2$).[8,9] Moreover, even the choice of electrolytes, binders, and separators also affects the overall performance and safety of LIBs.[10–12]

Aqueous lithium-ion batteries (ALIBs) have gained significant interest as a safer, more environmentally friendly alternative to conventional lithium-ion batteries for some applications, due to their utilization of water-based electrolytes.[13] The combination of lithium manganese oxide ($LiMn_2O_4$) cathodes and iron phosphate ($FePO_4{\cdot}2H_2O$) anodes has shown promising electrochemical performance and stability.[14] Alternative materials, such as lithium iron phosphate ($LiFePO_4$) cathodes and vanadium or titanium-based anodes among others, have also been explored for their potential in ALIBs.[15]

When it comes to 3D printing techniques, a plethora of methods have been explored for fabricating LIBs,[16–18] including fused deposition modeling (FDM), selective laser sintering (SLS), vat polymerization or stereolithography (SLA),[19,20] direct ink writing (DIW), and aerosol jet printing (AJP).[5,7,21] Each technique has its advantages and limitations, which are contingent upon factors such as material compatibility, resolution, and printing speed.

Electrode design and active material choice are other critical aspects that dictate the performance of 3D printed LIBs. The configuration of electrodes, such as interdigitated, spiral, or coaxial designs, can significantly influence the electrochemical performance, energy density, and power density of the batteries. For instance, interdigitated electrodes offer shorter Li-ion diffusion pathways, which can enhance the rate capability of the batteries. Similarly, coaxial designs provide an efficient integration of anode and cathode materials, resulting in a higher volumetric energy density. Porous architected current collectors can improve active material loading ratio and utilization.[4,22–24]

Active materials, in conjunction with electrode configurations, play a vital role in determining the overall performance of LIBs. The selection of suitable active materials depends on factors such as specific capacity, voltage range, stability, and safety.[25] For example, the use of silicon as an anode material can significantly improve the specific capacity of LIBs, but its large volume change during lithiation and delithiation poses challenges in maintaining the mechanical integrity of the electrode.[9] On the other hand, lithium iron phosphate ($LiFePO_4$) cathodes offer improved safety and longer cycle life compared to conventional lithium cobalt oxide ($LiCoO_2$) cathodes but suffer from lower energy density and voltage.[26]

*Electrochemical Society Member.
zE-mail: c.odwyer@ucc.ie

Additive manufacturing of LIBs offers several advantages over traditional manufacturing methods. The ability to create complex geometries and customized designs allows for the development of batteries tailored to specific applications and space constraints. Also, 3D printing techniques enable the fabrication of precisely controlled microstructures, which can enhance the electrochemical performance of the batteries by optimizing ion and electron transport pathways.[23,27] Finally, AM can potentially reduce material waste and manufacturing costs by using only the required amount of material and eliminating the need for expensive molds and tooling.[7,28,29] It is important that AM methods can be used to build or deposit all LIB components: case, current collector, active materials, separators, and even electrolyte (gel or solid).[7,30–32] For these reasons, it is safe to say that additive manufacturing holds great potential in transforming the field of lithium-ion batteries by enabling the fabrication of customized, high-performance, and cost-effective energy storage devices,[33,34] and provides routes to structural batteries[35,36] that can be smaller sized or larger cells that are integrated into the physical and mechanical structure (e.g. panels) of what they power.

Despite the many advantages, there are also challenges associated with the additive manufacturing of LIBs that need to be addressed. One of the most significant challenges is the compatibility of 3D printing techniques with battery materials. Many conventional anode, cathode, and electrolyte materials are not readily processable using existing 3D printing methods, necessitating the development of new materials or modifications to the existing ones.[32,37,38] Moreover, the resolution and printing speed of some techniques may not meet the stringent requirements for fabricating high-performance LIBs with ultra-thin and homogeneous layers.[4,5] Additionally, ensuring the safety and reliability of 3D printed LIBs during operation remains a challenge, as the formation of dendrites and the occurrence of mechanical stresses can lead to capacity fading, internal short-circuits, and thermal runaway.[39]

In this paper, we report on the design, modeling and vat polymerization (Vat-P) 3D printing of coin type lithium-ion battery cases and current collectors. The 3D printed battery parts are demonstrated in aqueous and non-aqueous lithium-ion battery fabrication. Physical, microscopic, and electrochemical characterization of internal metallization of the current collectors and assembled 3D printed cells are also outlined. Issues encountered in the process of printed battery fabrication are described and addressed by evolution of the cell design and material modifications, and the basis for these changes are described. The energy storage performance of the new 3D printed devices has been evaluated. We present the evolution of cell design from the simple derivative of a conventional coin cell to a more advanced and versatile modular layout that is better suited for 3D printed Li-ion batteries.

Materials and methods

3D modeling of electrode and cell designs.—Three versions of coin type full cells with architected porous current collectors were designed using SideFX Houdini Apprentice software and exported as STL files. The version I (V1) cell was equipped with a 3D printed gasket, version II (V2) was gasketless with a monolithic current collector/case, and version III (V3) had separate current collector pieces attached to the case after metal coating (Fig. 1). The cells were modeled with a modified diamond cubic (DC) or body-centered cubic (BCC) microlattice current collector geometry (Fig. 2A). These ordered porous structures, which function as the current collectors, have two benefits: 1) they allow defined total volume recesses for active material slurry without contributing to the thickening of the cell. 2) each "pocket" of active material is surrounded by current collector ensuring good and equal electrical connectivity through each electrode to minimize any electrochemically inactive "dead weight" active slurry material for a given gravimetric/volumetric mass loading.

3D printing by stereolithographic vat polymerization.—The ordered porous current collector lattice was rotated in software as appropriate, and the topmost edges were flattened in software prior to printing to ensure good even contact between cathode and anode sides and the electrolyte-soaked separator. The STL models were processed using Formlabs PreForm slicer software—scaled, duplicated, and oriented in accordance with the printer instruction manual. Supports were automatically generated by software with manual editing where necessary. All cell parts were printed using Formlabs Form 2 desktop SLA 3D printer with 25 μm layer thickness.

Clear V4 and High Temp V2 methacrylate-based resins (Formlabs) were selected for printing due to their relatively good solvent resistance, High Temp V2 being also heat resistant, with full details of the resins shown in Table I. Upon completion of the printing, the objects attached to the build platform were rinsed at room temperature with isopropyl alcohol (IPA) in the Form Wash automated wash station to remove uncured resin. After washing, the parts were removed from the build platform, dried with an air blower, and post-cured in the Form Cure station (λ = 405 nm illumination, Formlabs) with the supports attached. Wash and post-cure parameters used are shown in Table II. Supports were carefully detached from the post-cured objects; the latter were polished using 800 and 1200 grit sandpaper to remove support touchpoint dents. After rinsing in IPA and drying, the current collector containing parts were fully coated with gold or nickel (nominal layer thickness 150–200 nm) using a Quorum Q150T S sputter coater equipped with a Ted Pella 57 × 0.1 mm Au or Ni target.

Materials and battery fabrication.—Iron phosphate dihydrate ($FePO_4{\cdot}2H_2O$), lithium manganese oxide ($LiMn_2O_4$, spinel, <0.5 μm particle size, >99%), N-Methylpyrrolidone (NMP, anhydrous, 99.5%), Poly(vinylidene fluoride) (PVDF), and lithium bis (trifluoromethanesulfonyl)imide (LiTFSI, anhydrous, 99.99% trace metals basis) were purchased from Sigma–Aldrich and used as received. Lithium cobalt oxide ($LiCoO_2$), graphite, Super-P carbon black and carboxymethyl cellulose—styrene-butadiene rubber binder (CMC-SBR, M.W. 400,000 g mol^{-1}) were purchased from MTI Corporation. Formlabs Clear Resin V4 (FLGPCL04) and High Temp resin V2 (FLHTAM02) were used for vat polymerization 3D printing. A 1.0 mol L^{-1} lithium hexafluorophosphate solution in ethylene carbonate/diethyl carbonate (50/50 v/v, Sigma–Aldrich) was used as electrolyte in non-aqueous batteries. Gorilla Epoxy two-component adhesive, Henkel Loctite hot melt glue gun sticks, and Prevest DenPro Fusion Flo light cured dental nano hybrid cement were tested as sealing materials for the cells. Whatman GF/D glass microfiber filters and Celgard 2325 PP/PE/PP trilayer membrane were used as separators in aqueous and non-aqueous batteries, respectively.

Anode and cathode material slurries for *aqueous* batteries were prepared by ball milling super-P carbon black with $FePO_4{\cdot}2H_2O$ (FPO) and $LiMn_2O_4$ (LMO), respectively, using a high-speed 3D ball mill (MTI corporation) with a maximum speed of 1200 rpm. Later, each powder was mixed with CMC–SBR and water suspension using a compact vacuum mixer (MTI corporation). The final slurry consists of 80% w/w active material (FPO or LMO), 10% Super P carbon black and 10% CMC–SBR binder with solid content ranging from 5%–10%. Ethanol was used to adjust the surface tension of the slurry mixture in order to make it spreadable inside the porous 3D substrates. Electrodes were prepared by drop casting each slurry into 3D printed Au-coated substrates and dried inside oven at 65 °C for 12 h. A gasket was attached where applicable (V1 cell), and a glass fibre separator (Whatman GF/D) was placed between cathode and anode parts (Fig. 1), 10 M LiTFSI aqueous electrolyte was added, and the resulting cell was sealed around the edges with one of the three tested sealants. The cross-section area of each 3D printed electrode was 3.14 cm^2 while the loading ratio between FPO-based anode and LMO-based cathode was 2.0. When the dental cement was used as a sealant, the initial curing was performed inside

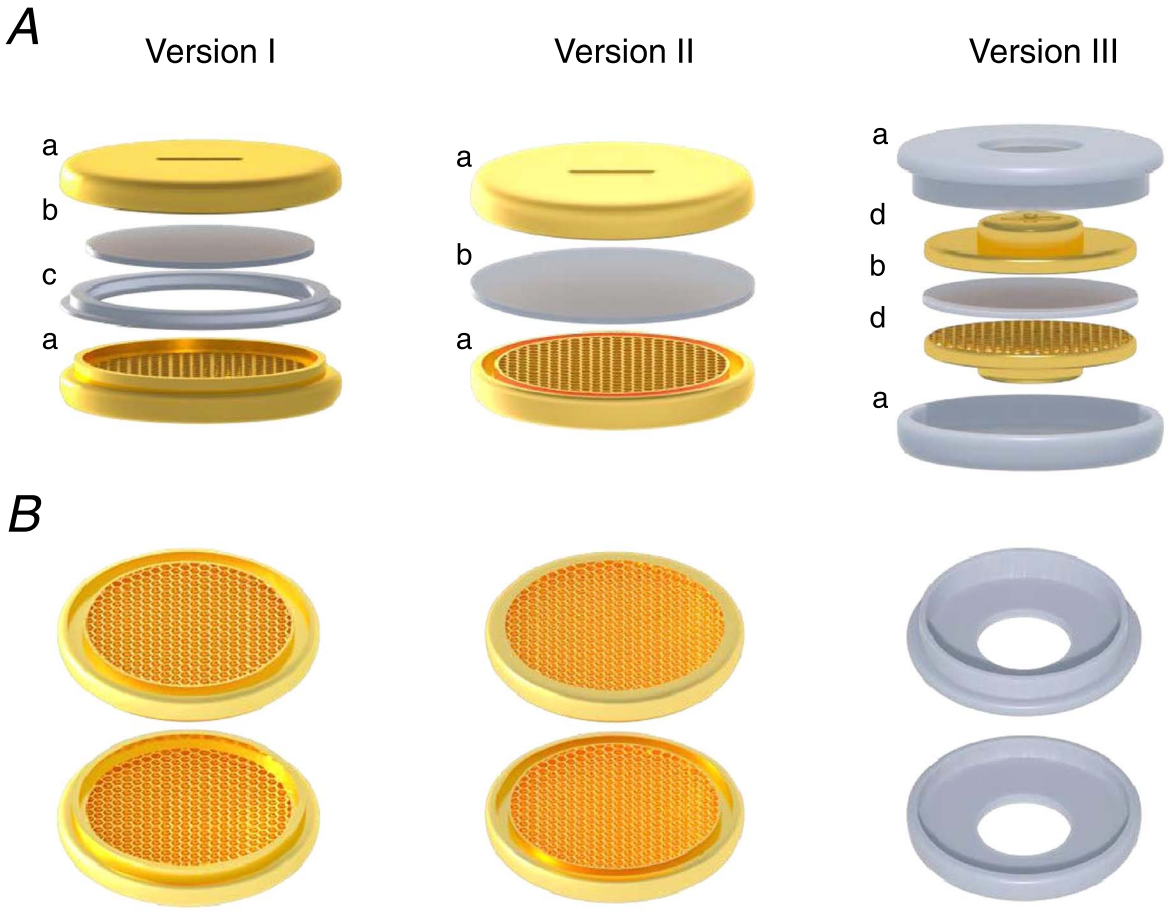


Figure 1. (A) Three versions of coin-type cell design evolution. The individual parts of each are (a) 3D printed case part. Version I and II have the porous current collector integrated into the outer casing, (b) separator, (c) 3D printed gasket (Version I only). (d) Version III uses a separate metallized current collector with non-metallized outer casing. (B) Top view of outer case parts for each cell version.

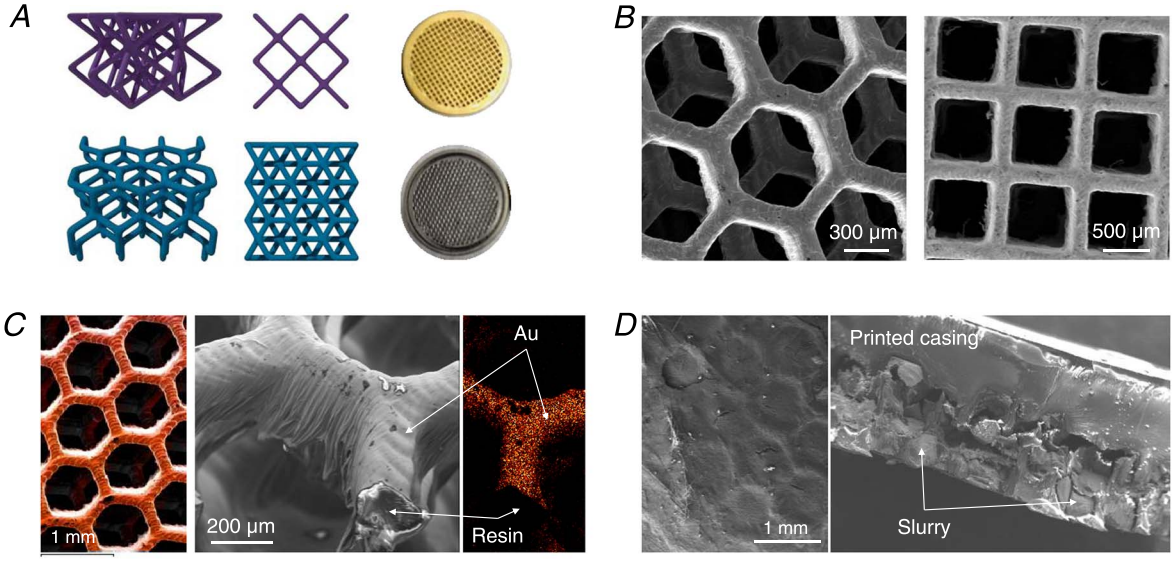


Figure 2. (A) 3D model of current collector lattice structures: body centered cubic (top row) and modified diamond cubic (bottom row). Side and top views of the structures (left and middle columns) and photographs of Version II metal-coated current collector cases (right column). (B) SEM images of DC (left) and BCC (right) current collectors. (C) EDX mapping of Au from SEM images of gold-coated DC current collectors. In the SEM image, the clear resin is coated by Au coating, the lower contrast is due to the Au conductivity; brighter internal features are from charging of the e-beam on more dielectric resin. (D) Plan view SEM of a $FePO_4$-filled current collector and cross-sectional image of the infilling of the material within the pores.

Table I. Solvent compatibility and heat resistance of Clear and High Temp resins. *Data corresponds to parts printed and post-cured with the parameters shown in Table II.

Property	Clear V4	High Temp V2
Heat Deflection Temp. @ 0.45 MPa*	73.1 °C	142 °C
Heat Deflection Temp. @ 1.8 MPa*	58.4 °C	99.2 °C
24 h Weight Gain (%) in Respective Solvent		
Acetone	sample cracked	<1
Isopropyl Alcohol	<1	<1
Sodium hydroxide (0.025%, pH = 10)	<1	<1
Diethyl glycol monomethyl ether	1.7	<1
Strong Acid (HCI Conc.)	distorted	1.2
Acetic Acid, 5%	<1	<1

Table II. Parameters of wash and post-curing steps.

Resin	Wash Duration, min	Post-cure Duration, min	Temperature, °C
Clear V4	10	15	60
High Temp V2	6	120	80

a glovebox (to avoid oxygen exposure) using a handheld LED UV torch ($\lambda = 395$ nm), then the assembled cells were additionally cured in the Form Cure curing device at room temperature for 5 min.

Active material slurries for *non-aqueous* cells were prepared similarly to the above procedure with a number of differences related to the non-aqueous nature of the system. Graphite and lithium cobalt oxide were used as an anode and cathode material, respectively; N-methylpyrrolidone and PVDF were used as a solvent and binder for the slurry preparation. The cathode material slurry composition (LCO:super P:binder) was 80:10:10 w/w/w. Anode material slurry contained graphite, binder (90:10 w/w) and solvent. Celgard 2325 membrane separator was cut in 16 mm diameter circles and placed between anode and cathode in non-aqueous batteries. Electrolyte addition (1 mol l^{-1} $LiPF_6$ in EC/DEC 1:1 v/v) and the final assembly of non-aqueous cells was performed inside a dry glovebox under Ar atmosphere (<0.1 ppm O_2/H_2O).

***Characterization and electrochemical testing.*—**The quality assessment of 3D geometric shapes was carried out using scanning electron microscope (SEM) images obtained with an FEI Quanta 650 SEM at spot size 3 and 20 kV beam voltage. Additionally, Energy Dispersive X-ray (EDX) analysis was employed to study the morphology and distribution of gold coating and the distribution of active material slurry within the pores of the current collector. Electrical conductivity evaluations were performed using a two-probe technique, and I − V data was gathered with a Keithley 2612B source meter at an integration time of 50 ms per point between 0 and 0.2 V. A consistent distance of 20 mm was maintained between the probes for all tests. Readings were taken across the porous side, the flat side, and between opposing planes of each electrode. Raman scattering analysis was performed on both uncoated and metal-coated electrode surfaces using a Renishaw InVia Raman spectrometer, equipped with a 30 mW Ar^+ laser at an excitation wavelength of 514 nm. A 40x lens was used to focus the laser, and a RenCam CCD camera collected the data.

Battery cycling and electrochemical measurements were performed using BioLogic VMP3 multichannel potentiostat controlled by EC-Lab software. Aqueous 3D printed cells in this study were cycled in the potential range of 0–1.3, 1.35, 1.4 V vs Li/Li^+ at various current densities in CC/CC or CCCV/CC modes (CC = constant current; CV = constant voltage). During the first formation cycle, non-aqueous batteries were charged to 4.0 V at 0.05 C constant current; the cycling was subsequently performed in the voltage range 3.0–4.2 V at various current densities in CCCV/CC mode.

Table III. Electric conductivity measurements for metal-coated V2 current collectors. Direction abbreviations correspond to the measurement across the porous side (A), the flat side (B), and between opposing planes of each electrode (C), i.e. thickness.

Metal coating	Lattice type	Direction	Resistance, Ohm
Gold	BCC	A	1.7
Gold	BCC	B	1.6
Gold	BCC	C	2.4
Gold	DC	A	2.4
Gold	DC	B	2.9
Gold	DC	C	2.1
Nickel	BCC	A	57
Nickel	BCC	B	29
Nickel	BCC	C	54
Nickel	DC	A	96
Nickel	DC	B	27
Nickel	DC	C	74

Results and Discussion

***Porous current collector imaging and physical characterization.*—**The suitability of nickel and gold as coating materials for 3D printed conductive substrates was tested. First, electrical conductivity measurements were performed on Au-coated and Ni-coated version II substrates, which showed that Au-coated substrates had significantly lower resistance (1.6–2.9 Ω) compared to Ni-coated substrates (29–96 Ω). Both clear and high temp resin substrates demonstrated very close conductivity results for all tested metal coating and lattice type combinations. For Au-coated substrates there was no noticeable difference observed between body centered cubic (BCC) and diamond cubic (DC) lattice. However, for Ni-coated substrates, DC lattice showed higher resistance than BCC lattice whenever one of the terminals was connected to the porous substrate (Table III).

The results suggest that Au-coated substrates provided better electrical conductivity compared to Ni-coated current collectors. The Au-coated substrates were also found to be significantly more stable after immersion in 10 M LiTFSI based aqueous electrolyte for 24 h. Raman scattering and imaging measurements showed negligible change to the resistance values of Au-coated substrates before and after electrolyte treatment, whereas Ni-coated substrates practically became significantly more resistive and in regions where delamination of Ni occurred, were non-conductive. Finally, it was observed that there was no significant difference in resistance for Au-coated substrates printed from two different polymer resins.

High resolution SEM images along with EDX analysis were used to examine the nickel and gold coating on the surface of polymer

substrates (Fig. 2B). It was observed that both nickel and gold completely covered the surface of the substrates and on the surfaces within each of the pores to ensure electrical connection with the infilled slurry material. For all tests in each version of the cell reported here, Au-coated porous current collectors with DC porous internal geometry were used.

EDX analysis of the current collector showed the uniform metallization by Au, shown in Fig. 2C. Comparison of scanning electron microscopy (SEM) images of the cross-sectional view of gold-coated substrate before and after the introduction of cathode material reveal a tightly packed arrangement of active material throughout the lower layers of the porous 3D electrode, and relatively uniform overcoat of the slurry across the infilled porous current collector, as shown in Fig. 2D.

Design and 3D printing of coin cell parts: rationale for material choice and model modifications.—In aqueous systems, both printing resins (clear and high temp) exhibited equally good electrolyte resistance with the testing results independent of the resin type. However, in the case of non-aqueous batteries, only the high temp resin was stable enough to maintain the shape and integrity of electrodes throughout the cell preparation procedure. The reason is that cathode material slurry contained N-methyl-2-pyrrolidone, which caused swelling of the clear resin polymer (summarized in Table II), but did not affect the high temp resin. Additionally, the electrode preparation in the case of non-aqueous systems involved solvent evaporation at higher temperatures than in the case of aqueous cells. These reasons dictated the choice of resins for fabrication of aqueous and non-aqueous batteries: the former were predominantly printed with clear resin, the latter were assembled using high temp prints only.

Version I design was inspired by a conventional coin cell structure with an insulating gasket placed between cathode and anode current collectors (Fig. 1A). Photos of 3D printed Version I cells parts are shown in Fig. 3. After preliminary tests with the aqueous Li-ion system it was found that although the gasket did perform as a good insulator, it also introduced three major challenges. The first issue was the brittleness of both types of cured resins used for printing. The printed gasket walls were relatively thin and easily broke upon such handling operations as detaching from supports and assembly of the cells. The cell case parts also occasionally cracked during cell assembly when some additional pressure was applied during assembly of the entire battery and all its parts.

The second issue with models that use separate gaskets was the limitation of Vat-P 3D printing resolution, which puts a lower limit on the thickness of some case elements and the gasket. This leads to an larger overall size of the assembled cell and a large unutilized overall volume. Finally, even Vat-P 3D printing, which is considerably better in render quality and resolution compared to fused deposition modelling (FDM for example), has limitations due to imperfections and small size variations in the resulting prints. When practitioners use this printing method, care should be taken to inspect the prints to avoid large and uneven electrode gaps, poor sealing, and difficulties in the gasket/case fitting. We managed to assemble and test several Version I batteries using aqueous chemistry. The electrochemical testing results are presented in Figs. 4 and 5, to be discussed later. That said, the aforementioned issues prevented any further testing of the V1 cells, and some modifications were applied in the Version II design.

The Version II printed coin cell was designed to be assembled without a separate printed gasket. In doing so, several printing and assembly issues were remedied including all the gasket supporting elements. A separator was used as an electronic insulator instead (Fig. 1A). By implementing this change, we were able to significantly decrease the cell thickness and overall coin cell volume and weight, leaving the electrode area almost unchanged. Reducing the number of elements considerably simplified the handling and assembling procedures of each cell.

As discussed earlier, a sputtered nickel coating proved to be readily oxidized in air, which reduced the surface conductivity by an order of magnitude. For this reason, the majority of electrochemical cycling tests were conducted with gold-coated current collectors only, which are stable both in air and at the cycling conditions in both electrolytes in their respective voltage ranges. Several Version II aqueous lithium-ion batteries were assembled and cycled. The electrochemical results are discussed in below. Despite the successful testing Version II with aqueous electrolytes, all attempts to achieve even a single charge/discharge cycle in non-aqueous electrolytes failed. Post-mortem analysis showed that the main reason for the failure was the exfoliation of the gold coating at the edges of the case/current collector and contact areas under the influence of a relatively low-viscosity organic electrolyte solution. There was an apparent exfoliation and thinning of the gold layer around the cell's outer regions after the addition of electrolyte. To implement a Vat-P printed cell that was stable in both aqueous and organic electrolytes, the Version III cell design was conceived. In this version, current collectors are separated from the rest of the case, and a circular wall is added to one of the case parts in order to improve sealing (cf Fig. 1A). The electrode surface area is slightly reduced in Version III cells. This approach allows us to reduce the amount of metal used for coating, avoid any contact between the gold coating during the cell assembly, and improve cell sealing. With the Version III layout we were able to successfully cycle the cells in both aqueous and non-aqueous batteries, as we be discussed in the next section.

In developing resin or plastic-based rechargeable aqueous and non-aqueous Li-ion batteries, new issues emerge when the plastic needs to be engineered or modified to maintain, as close as possible, some useful attributes of metal casings. While polymeric casings are much lighter and benefit overall cell-level energy density, polymer 3D printed cases cannot usually withstand high pressure and can crack during assembly or charging. This was the case with Version I and Version II designs during our testing. In the absence of a conductive resin that at the time of writing is not available, the design is limited by a conductive surface coating. Coating integrity is a function of geometric complexity in printed design and can potentially create lower electrically conductive pathways at the high-curvature regions due to erosion by electrolyte and lower accessibility during vapor or electroless deposition. However, modifications outlined for Version III were successful overall for both aqueous and non-aqueous rechargeable cells.

Since 3D printed cells cannot be crimped or compressed like coin cells during assembly, alternative sealing methods need to be developed to maintain structural integrity, avoid electrolyte leakage and evaporation, and to prevent outside atmosphere ingress particularly for organic electrolyte containing cells. We did extensive testing of three different sealants: (1) epoxy resin, (2) EVA hot-melt adhesive, and (3) uv-cured dental hybrid cement. The best performance was achieved with dental cement due to its extremely high strength and solvent resistance, as well as excellent adhesive properties. In order to avoid the formation of oxygen-inhibited layer, the sealing is best performed in an oxygen-free atmosphere. The option to use the same uncured resin as a sealant was ruled out because of insufficient viscosity of the resin.

Inexpensive EVA adhesives have a low creep resistance[40] and a poor adhesion to the photopolymerized PMMA-based resins used for printing, which adversely impacted the sealing quality and limited their application in our experiments. Hot-melt adhesive requires a significant time to cool and solidify after application. This can make it challenging to achieve consistent and reliable seals. Additionally, EVA hot-melt glue has poor solvent and chemical resistance to organic electrolytes and active compounds used in lithium-ion batteries. Plasticizers used in the glue compositions may contaminate the electrolyte and cause battery performance degradation.

While the epoxy glue adhesive demonstrated reasonably good sealing quality in aqueous systems and strong adhesion to the cell surface, it had some drawbacks in non-aqueous batteries such as

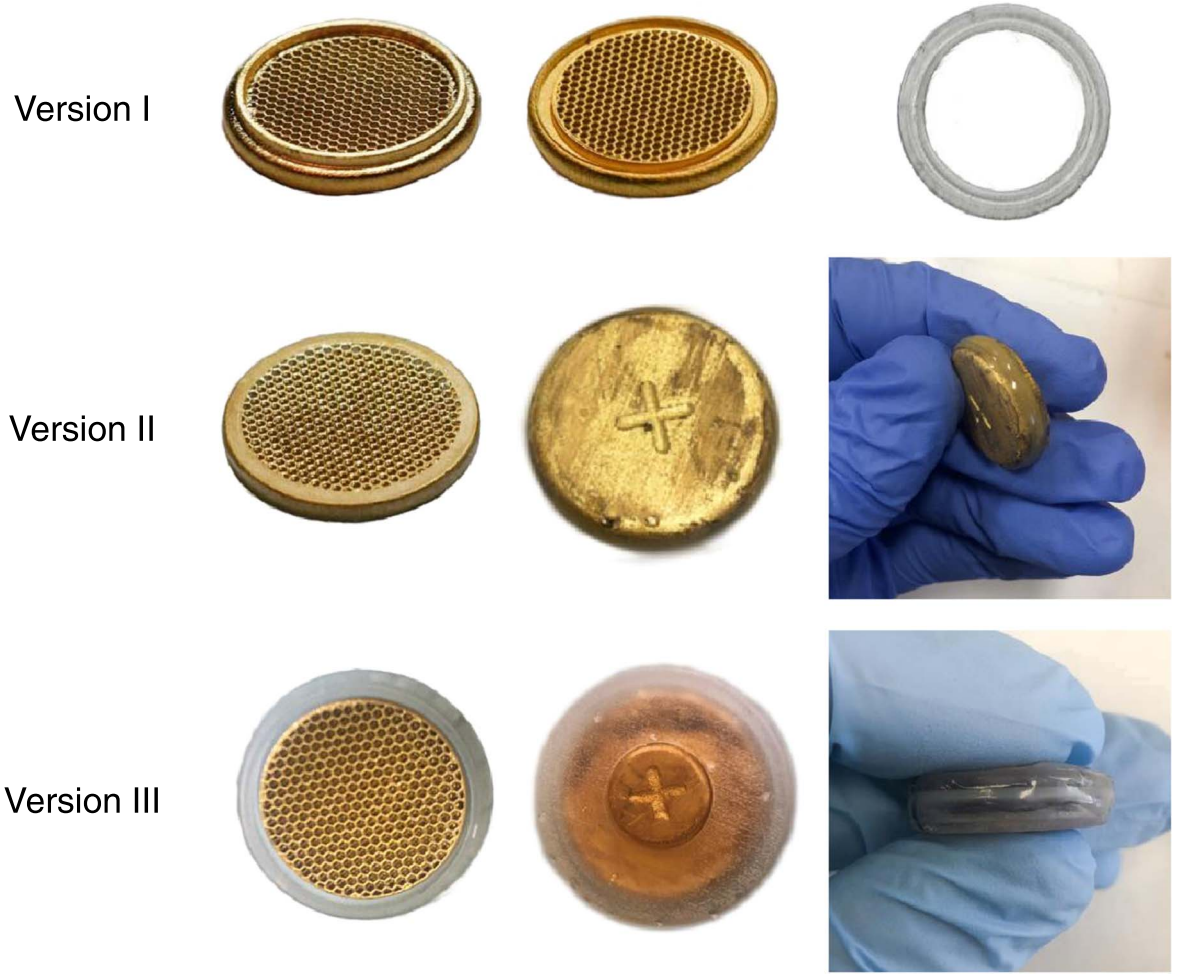


Figure 3. Photographs of different versions of 3D printed cell parts and assembled cells. Issues common to these designs such as breakage, delamination, and cracking are shown that led to the final design, assembling and sealing method to render a stable cell.

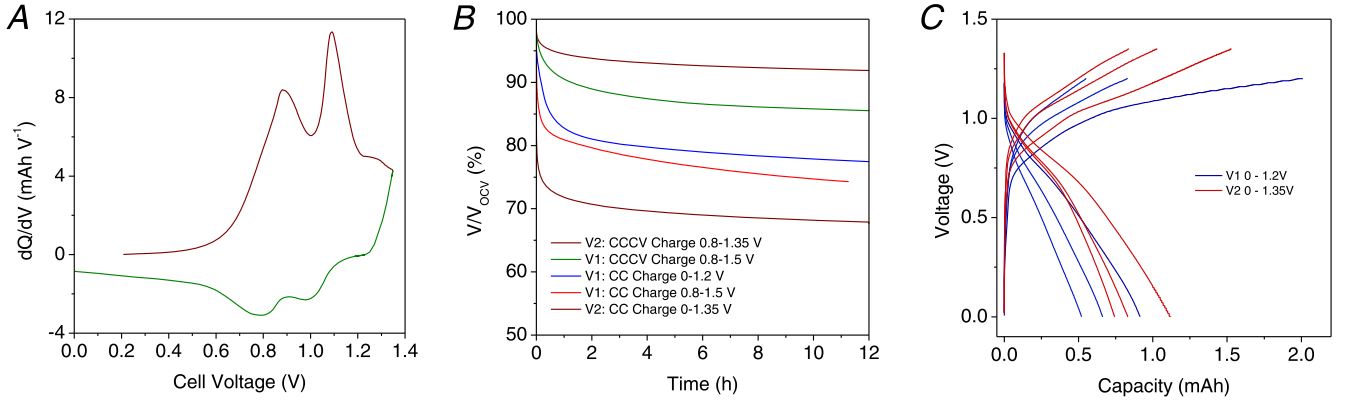


Figure 4. (A) Differential capacity (dQ/dV) plot for Version I aqueous Li-ion cell. (B) Measured change in OCV over time for different versions of the 3D printed batteries and for different charging modes. (C) First 3 charge/discharge cycles for Version I and Version II cells.

limited resistance to organic solvents, relatively long curing time, and sensitivity to component mixing ratio. Also, the components of epoxy resin can contaminate organic electrolytes, deteriorate the battery performance, and ultimately lead to its failure. Epoxy glues can become brittle over time, which may lead to seal failure and potential leaks. The ceramic-based dental resin, once cured, was a very effective and consistent sealant for 3D printed coin cells for aqueous and non-aqueous internal chemistry.

Electrochemical testing of Vat-P 3D printed coin cells.—All of the designs of Vat-P printed coin cell batteries discussed above were electrochemically tested using at least one kind of Li-ion battery chemistry (aqueous or non-aqueous). Due to the limitations of some materials discussed above, the first two versions (Version I and Version II) were cycled as aqueous cells only.

The electrochemical behavior and performance of 3D printed Li-ion batteries was tested using galvanostatic charge/discharge cycling

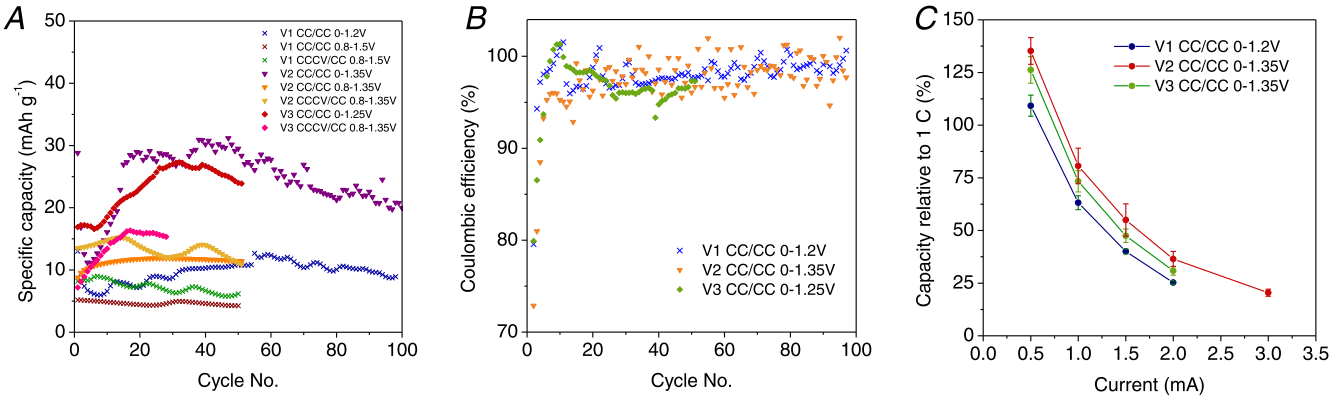


Figure 5. (A) Specific discharge capacity for different cell versions and cycling conditions in aqueous system, factoring the mass of the entire assembled cell including all components and materials. (B) Coulombic efficiency for different cell versions in aqueous systems. (C) Rate capability test demonstrating capacity change at different discharge currents.

Table IV. Comparison of performance characteristics of coin cell and 3D printed cells.

Performance Metrics	Metal Coin Cell	Version I	Version II	Version III
Specific Capacity, mAh g^{-1}	100	12	30	27
Gravimetric Capacity/Cell, mAh g^{-1} a)	0.51	0.53	1.45	1.14
Volumetric Capacity/Cell, mAh cm^{-3}	1.53	0.73	1.98	1.67
Energy Density/Cell, Wh kg^{-1} b)	0.51	0.53	1.45	1.14

a) Mass of metal cell 2.98 g; masses of 3D printed cells 1.47, 1.34, 1.53 g (I, II, III). b) Nominal voltage 1.0 V.

in constant current/constant voltage (CCCV) or constant current (CC) charging mode. Differential capacity plots obtained from the galvanostatic charge-discharge curves for the 3D printed Li-ion battery showed two prominent pairs of oxidation and reduction peaks (Fig. 4A). These peaks represent the lithiation and delithiation of the anode $FePO_4$ and cathode $LiMn_2O_4$, respectively, and can be attributed to two reversible electrochemical reactions: $2Li_{0.5}Mn_2O_4 + Li^+ + e^- \leftrightarrows 2LiMn_2O_4$ and $4MnO_2 \leftrightarrows 2Li_{0.5}Mn_2O_4 + Li^+ + e^-$.[41]

Discharging was performed at constant current in all cases. Self-discharge of the charged cells was evaluated by measuring the variation of the open circuit voltage (OCV) for 12 h. This measurement is important for 3D printed cells and cells made from non-traditional current collector geometries and materials to quantify the stability of the cell at a high state of charge. The results are summarized in Fig. 4B. As can be seen, in the case of CC charging, a rapid and deep decline in the cell voltage is observed, which indicates that chemical and diffusion processes tend to equilibrium for some time after the charging ends. This can be due to the increased thickness of active material layers inside the cell, hence the kinetic delay in reaching equilibrium. Nevertheless, this quite significant drop in the cell voltage (>20%) translates to less than 5% drop in capacity of the battery in the case of the Version I cell charged to 1.2 V. Utilizing CCCV charging mode (0.8–1.35 V; 0.8 V—1.5 V) significantly improved self-discharge behavior, where both Version I and Version II cells maintained 86% and 92% of OCV after 12 h. This charging method allows better utilization of active material and accelerating transition to the equilibrium state.

Figure 4C shows the first 3 cycles charge/discharge profiles for different versions of aqueous coin cell. The profile shape is in good agreement with the literature data[14] for this aqueous system in standard-type cells, as a function of the capacity of the entire cell, not just the specific capacity of one of the electrode active materials. The cells are very stable, and we note an improvement overall in a larger voltage window up to 1.35 V. Specific discharge capacity and coulombic efficiency plots for all cell versions with the aqueous electrolyte in different voltage cutoff ranges are summarized in Figs. 5A, 5B. In general, the specific capacity of the cell briefly increases during first several cycles reaching peak values of 12, 30, and 27 mAh g^{-1} for Versions I, II and III cells, respectively. However, a steady decay in cell capacity is observed after 30th–50th cycle. Low coulombic efficiencieds obtained in the first several cycles of the 3D printed battery could indicate the intensive formation of SEI layers inside its highly porous 3D architecture, since none of the material were prelithitated or electrochemical preconditions prior to use at the stable cycling voltage. After several initial formation cycles, coulombic efficiency tends to 95%–100%, which indicates the reversible nature of electrochemical processes during charge/discharge cycling at this stage. Gradual increase in capacity can be explained by the fact that thick and porous 3D electrode allows complete utilization of active material, but there are kinetic limitations due to the thickness of the electrodes and the volume of material in each of the current collector pores. As the cycling proceeds, more material is available for lithiation and delithiation, thus increasing the capacity. Once the capacity of the cell achieved the maximum value, it remains stable for a prolonged cycling period before gradual decline. We believe that the performance levels of the 3D printed Li-ion batteries with thick, porous electrodes we show here do not fully showcase their true capability and are an unoptimized lower bound. Additional research and advancements are necessary to fully harness the potential of the active materials in these types of cells.

The design ensures that the conductivity of 3D printed porous electrodes is improved and behaves as a metallic coin cell casing in this regard. This was also confirmed using rate capability testing (Fig. 5C). The shape of the plots was almost independent on the battery version and was defined by the active material composition and current collector geometry (which was the same in all cell versions). We suggest that the good rate capability of 3D printed lithium-ion aqueous batteries is the result of highly interconnected network that provides multiple pathways for electronic conductivity within the porous current collector.

Table IV presents a comparison of the performance characteristics for both conventional and 3D printed aqueous lithium-ion cells featuring FPO/LMO active materials. When considering gravimetric capacities (based on the total mass of the cell), the 3D printed cell surpasses the traditional coin cell. This is because the 3D printed

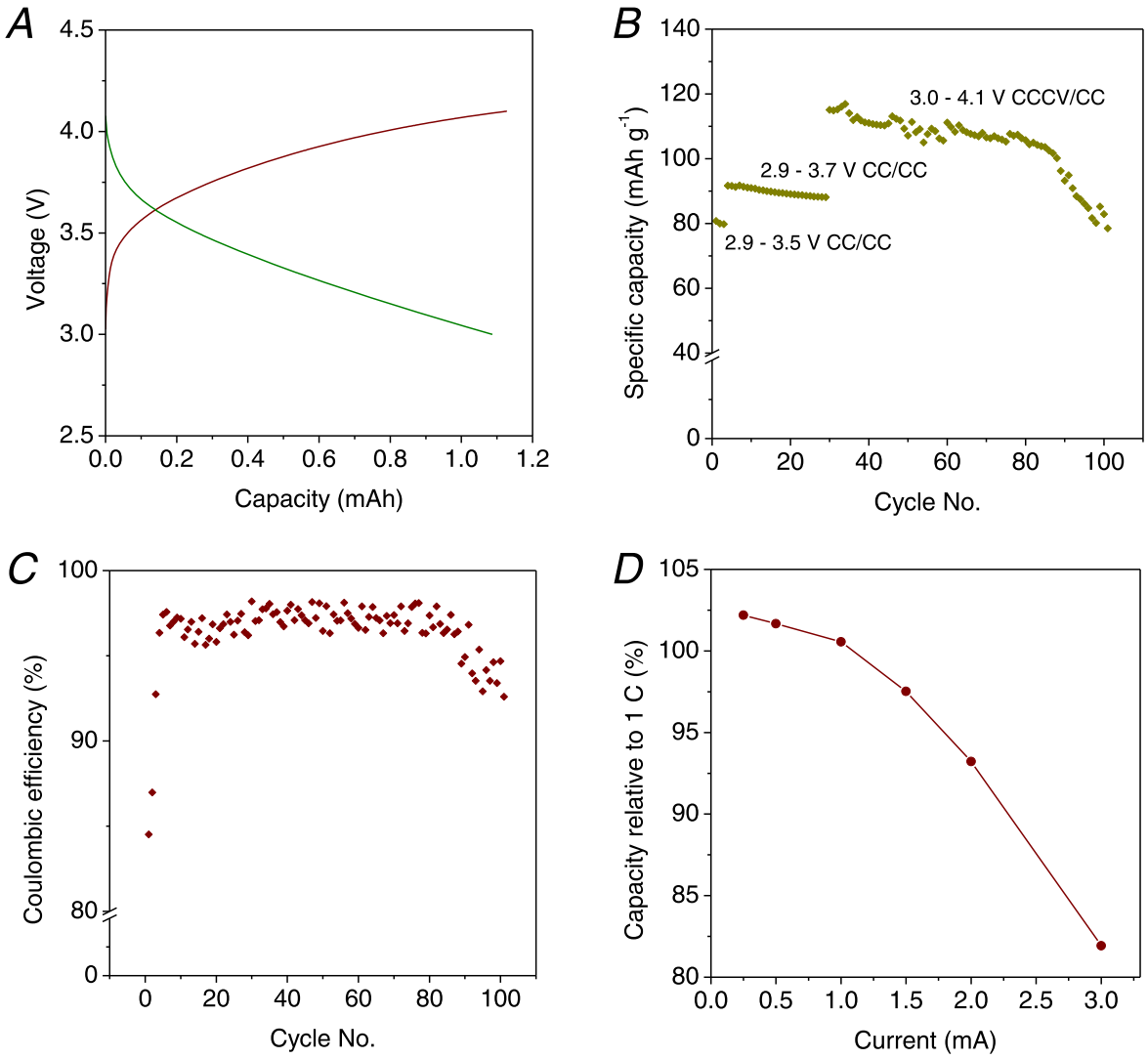


Figure 6. (A) Charge/discharge profile for Version III non-aqueous LIB (3rd cycle). (B) Specific discharge capacity of Version III non-aqueous battery in different cycling modes vs cycle number. (C) Coulombic efficiency for the cycling test shown in Fig. 6B. (D) C-rate performance of the same cell.

lithium-ion cells are approximately half the weight and deliver higher capacities at elevated rates. However, when dense and thick electrodes are used in the 3D printed aqueous, it can restrict the full use of the active material, possibly due to inadequate wetting of the 3D printed electrode.

Internal resistance measurements once again confirmed the advantage of the Version III design compared to Version I and Version II. The average internal resistance for aqueous batteries was 3.2 ± 0.8 Ω (Version I), 3.2 ± 0.8 Ω (Version II) and 0.4 ± 0.3 Ω (Version III). As mentioned above, non-aqueous 3D printed cells using carbonate-based electrolytes were successfully assembled and tested using the Version III cell design only. The electrochemical response is presented in Fig. 6. The results show that Version III 3D printed coin cells reached the specific capacity of ∼115 mAh g^{-1} caculated using the mass of the LCO active materials, which is only ∼20% less than the maximum reversible capacity of $LoCoO_2$.[42] The entire cell itself delivered ∼1.14 mAh g^{-1}.

The capacity per unit footprint area was higher for the 3D printed cells than for conventional coin cells due to the increased surface area and three-dimensional structure of the porous current collector. Similar to the aqueous batteries, the gravimetric capacity per unit mass of the assembled cell (∼12 mAh cm^{-2}) was higher than for conventional coin cells (∼8–10 mAh cm^{-2}) due to the low case material density. Rate capability measurement results showing the capacity relative to the capacity at a rate of 1 C were on par with conventional LCO coin cells (Fig. 6D). Although the maximum achieved specific capacity was somewhat lower than the theoretical capacity of LCO material, we believe that the performance of Vat-P or SLA 3D printed batteries can be significantly improved, and it already compares well compared to coin cells using LCO with graphite anode material. The response reported here constitutes the state of the art for non-aqueous Vat-P printed cells using these electrode materials.

Conclusions

In this work, we described the design, modeling and vat polymerized SLA 3D printing of coin cell-type lithium-ion battery cases and current collectors. Three different versions of the battery design were proposed, and the evolution from the first concept to the final working prototypes was outlined. We explained the rationale behind each modification that allowed us to improve the performance, handling and assembly of the printed batteries. Some guidance into the modeling, 3D printing process, material choice, and performance of 3D printed Li-ion batteries was provided.

We conducted physical and electrochemical characterization of the printed cells and studied the characteristics of gold and nickel PVD coating of the 3D printed current collectors. Gold-coated

substrates outperformed nickel-coated ones in terms of electrical conductivity and resistance to solvent erosion. SEM and EDX images confirmed the full substrate metal coating and a high active material infill of the porous current collectors.

Different kinds of sealing adhesives were studied: two-component epoxy resin, hot melt adhesive, and uv-cured dental cement. The best results were achieved with cured cement due to its adhesive properties and electrolyte resistance. Epoxy resin demonstrated an average sealing and handling quality, and good adhesive properties. Finally, the low-cost hot melt adhesive was the least suitable in our tests mainly due to its low creep resistance and long setting time leading to poor adhesion to the surface and electrolyte leaks.

Electrochemical tests such as charge/discharge cycling, self-discharge monitoring, and rate capability assessment were performed for all three versions of design in aqueous system. The final version III cell was also tested with non-aqueous chemistry, being the only working version suitable for an organic-electrolyte Li-ion battery. We found that 3D printed Li-ion batteries demonstrated promising results in terms of gravimetric capacity, rate capability, and capacity per unit footprint area compared to conventional coin cells in both aqueous and non-aqueous systems. For example, the Version III 3D printed non-aqueous coin cell achieves the specific capacity of 115 mAh g^{-1}, which is only ∼20% less than the maximum reversible capacity of LCO and provides a cell-level capacity of over 1 mAh g^{-1} compared to ∼0.5 mAh g^{-1} for a metal coin cell using identical internal components and materials.

Despite the challenges faced in optimizing the design and materials for 3D printed Li-ion batteries, this study provides valuable information for future research and development. Additional research and advancements are necessary to fully utilize the capacity of the active materials in this type of cells and improve the performance of SLA 3D printed batteries, notably the fine tuning of current collector porosity, pore depth, active material mass loading and thickness and obtaining thinner, lighter cells without mechanical issues caused by fundamental limitation of thickness and rigidity of some photopolymerized resins. In conclusion, 3D printed Li-ion batteries hold significant promise for the future of energy storage technology, offering potential advantages in terms of engineering speed, cost, weight, capacity, adaptability, and these cells could also potentially be recycled by combustion, significantly impacting the issues of single use and disposable small cell battery accumulation and recycling.

Acknowledgments

Support is also acknowledged from the European Union's Horizon 2020 research and innovation program under grant agreement No 825114. This work is partly supported by Enterprise Ireland Commercialisation Fund as part of the European Regional Development Fund under contract no. CF-2018–0839-P. Supporting from the Irish Research Council under an Advanced Laureate Award (IRCLA/19/118) and Government of Ireland Postdoctoral Fellowship (GOIPD/2021/438) are gratefully acknowledged.

ORCID

Colm O'Dwyer https://orcid.org/0000-0001-7429-015X

References

1. B. Dunn, H. Kamath, and J.-M. Tarascon, *Science*, **334**, 928 (2011).
2. T. M. Gür, *Energy Environ. Sci.*, **11**, 2696 (2018).
3. I. Gibson, D. W. Rosen, and B. Stucker, *Additive Manufacturing Technologies: Rapid Prototyping to Direct Digital Manufacturing*, ed. I. Gibson et al. p. 378 (Springer, US, Boston, MA) (2010).
4. F. Zhang, M. Wei, V. V. Viswanathan, B. Swart, Y. Shao, G. Wu, and C. Zhou, *Nano Energy*, **40**, 418 (2017).
5. A. Zhakeyev, P. Wang, L. Zhang, W. Shu, H. Wang, and J. Xuan, *Adv. Sci.*, **4**, 1700187 (2017).
6. Y. Yang, W. Yuan, X. Zhang, Y. Yuan, C. Wang, Y. Ye, Y. Huang, Z. Qiu, and Y. Tang, *Appl. Energy*, **257**, 114002 (2020).
7. V. Egorov, U. Gulzar, Y. Zhang, S. Breen, and C. O'Dwyer, *Adv. Mater.*, **32**, 2000556 (2020).
8. B. L. Ellis, K. T. Lee, and L. F. Nazar, *Chem. Mater.*, **22**, 691 (2010).
9. M. Armand et al., *J. Power Sources*, **479**, 228708 (2020).
10. P. Arora and Z. Zhang, *Chem. Rev.*, **104**, 4419 (2004).
11. Y. Liu, Y. Qiao, Y. Zhang, Z. Yang, T. Gao, D. Kirsch, B. Liu, J. Song, B. Yang, and L. Hu, *Energy Storage Mater.*, **12**, 197 (2018).
12. K. Xu, *Chem. Rev.*, **114**, 11503 (2014).
13. Y. Liang and Y. Yao, *Nature Reviews Materials*, **8**, 109 (2023).
14. Y. Wang et al., *ACS Appl. Mater. Interfaces*, **10**, 7061 (2018).
15. Y. Wang, J. Yi, and Y. Xia, *Adv. Energy Mater.*, **2**, 830 (2012).
16. S. D. Lacey et al., *Adv. Mater.*, **30**, 1705651 (2018).
17. J. Li, M. C. Leu, R. Panat, and J. Park, *Mater. Des.*, **119**, 417 (2017).
18. Z.-X. Low, Y. T. Chua, B. M. Ray, D. Mattia, I. S. Metcalfe, and D. A. Patterson, *J. Membr. Sci.*, **523**, 596 (2017).
19. U. Gulzar, V. Egorov, Y. Zhang, and C. O'Dwyer, *Advanced Energy and Sustainability Research*, **4**, 2300029 (2023).
20. A. C. Martinez et al., *Sci. Rep.*, **12**, 19010 (2022).
21. U. Gulzar, C. Glynn, and C. O'Dwyer, *Current Opinion in Electrochemistry*, **20**, 46 (2020).
22. V. Egorov and C. O'Dwyer, *Current Opinion in Electrochemistry*, **21**, 201 (2020).
23. K. Sun, T.-S. Wei, B. Y. Ahn, J. Y. Seo, S. J. Dillon, and J. A. Lewis, *Adv. Mater.*, **25**, 4539 (2013).
24. S. H. Park, M. Kaur, D. Yun, and W. S. Kim, *Langmuir*, **34**, 10897 (2018).
25. J. B. Goodenough and K.-S. Park, *J. Am. Chem. Soc.*, **135**, 1167 (2013).
26. A. K. Padhi, K. S. Nanjundaswamy, and J. B. Goodenough, *J. Electrochem. Soc.*, **144**, 1188 (1997).
27. Y. Li, Z.-Y. Fu, and B.-L. Su, *Adv. Funct. Mater.*, **22**, 4634 (2012).
28. X. Shi, Z.-S. Wu, and X. Bao, *Electrochemical Energy Reviews*, **3**, 581 (2020).
29. C. Reyes, R. Somogyi, S. Niu, M. A. Cruz, F. Yang, M. J. Catenacci, C. P. Rhodes, and B. J. Wiley, *ACS Appl. Energy Mater.*, **1**, 5268 (2018).
30. X. Gao, M. Zheng, X. Yang, R. Sun, J. Zhang, and X. Sun, *Mater. Today*, **59**, 161 (2022).
31. S. Ponnada, D. Babu Gorle, R. S. Chandra Bose, M. Sadat Kiai, M. Devi, C. Venkateswara Raju, N. Baydogan, K. Kar Nanda, F. Marken, and R. K. Sharma, *Batteries & Supercaps*, **5**, e202200223 (2022).
32. D. W. McOwen et al., *Adv. Mater.*, **30**, 1707132 (2018).
33. P. Chang, H. Mei, S. Zhou, K. G. Dassios, and L. Cheng, *J. Mater. Chem. A*, **7**, 4230 (2019).
34. X. Tian, J. Jin, S. Yuan, C. K. Chua, S. B. Tor, and K. Zhou, *Adv. Energy Mater.*, **7**, 1700127 (2017).
35. L. E. Asp, M. Johansson, G. Lindbergh, J. Xu, and D. Zenkert, *Functional Composites and Structures*, **1**, 042001 (2019).
36. L. E. Asp et al., *Advanced Energy and Sustainability Research*, **2**, 2000093 (2021).
37. J. Wang et al., *ACS Appl. Mater. Interfaces*, **10**, 39794 (2018).
38. E. Strauss, S. Menkin, and D. Golodnitsky, *Printed Batteries: Materials, Technologies and Applications* p. 80 (Wiley, New York) (2018).
39. X.-B. Cheng, R. Zhang, C.-Z. Zhao, and Q. Zhang, *Chem. Rev.*, **117**, 10403 (2017).
40. N. Ercan and E. Korkmaz, *Mater. Today Commun.*, **28**, 102634 (2021).
41. A. V. Potapenko and S. A. Kirillov, *J. Energy Chem.*, **23**, 543 (2014).
42. Q. Wu, B. Zhang, and Y. Lu, *J. Energy Chem.*, **74**, 283 (2022).